AGU PUBLICATIONS

JGR

Journal of Geophysical Research: Atmospheres

RESEARCH ARTICLE
10.1002/2016JD025764

Key Point:
- Subtropical cyclones over subtropical South Atlantic develop with a tropical moisture source

Correspondence to:
L. F. Gozzo,
luizfelippeg@fc.unesp.br

Citation:
Gozzo, L. F., R. P. da Rocha, L. Gimeno, and A. Drumond (2017), Climatology and numerical case study of moisture sources associated with subtropical cyclogenesis over the southwestern Atlantic Ocean, *J. Geophys. Res. Atmos.*, *122*, 5636–5653, doi:10.1002/2016JD025764.

Received 9 AUG 2016
Accepted 17 MAY 2017
Accepted article online 25 MAY 2017
Published online 5 JUN 2017

©2017. American Geophysical Union. All Rights Reserved.

Climatology and numerical case study of moisture sources associated with subtropical cyclogenesis over the southwestern Atlantic Ocean

L. F. Gozzo[1,2], R. P. da Rocha[2], L. Gimeno[3], and A. Drumond[3]

[1]Departamento de Física, Universidade Estadual Paulista and Centro de Meteorologia de Bauru (IPMET), Bauru, Brazil, [2]Departamento de Ciências Atmosféricas, IAG, Universidade de São Paulo, São Paulo, Brazil, [3]Ephyslab, Facultad de Ciencias, Universidad de Vigo, Ourense, Spain

Abstract An important feature during cyclogenesis is the availability of moisture to fuel the associated convective activity providing faster developments and more intense systems. In this work, an investigation of the role of local evaporation and remote water vapor transport prior to subtropical cyclogenesis in the southwestern South Atlantic (named RG1 region) is presented. Results were obtained analyzing the period from 1980 to 2015 with a Lagrangian particle dispersion model together with the ERA-Interim reanalysis. The northern sector of the Subtropical High in the South Atlantic Ocean stands out as the main source region of water vapor to the RG1, with the low-level northeasterly winds being responsible by moisture transport. An anomalous moisture transport from lower latitudes preceded the subtropical cyclogenesis events and provided the necessary water vapor to fuel the convective activity. A numerical case study using the Weather Research and Forecasting mesoscale model indicated that the remote moisture source is essential for subtropical cyclogenesis in RG1, since it allows a stronger surface low pressure to develop and supports the formation of a cutoff low in the middle troposphere. Though the local evaporation has a secondary role in this process, it helped the system to attain the observed intensity and subtropical characteristics. Therefore, both local and remote moisture sources provide the incipient subtropical cyclone with the horizontal temperature advection and convective activity necessary to its further development.

1. Introduction

Subtropical cyclones are nonfrontal low-pressure systems with a thermally hybrid core (warm at low levels and cold at upper levels) and intense convective activity that develop mostly over the oceanic areas. Their occurrence over South America, more specifically in the southwestern South Atlantic, is documented in a number of case studies [*McTaggart-Cowan et al.*, 2006; *Veiga et al.*, 2008; *Pereira-filho et al.*, 2010; *Vianna et al.*, 2010; *Dias Pinto et al.*, 2013], and the climatology of such systems is presented in *Evans and Braun* [2012] and *Gozzo et al.* [2014]. This is still an incipient research area, and a better comprehension of subtropical cyclone (SC) development is important in a theoretical point of view and also to improve operational weather forecast. The predictability of SCs in South America is low: their forecast and representation are poor in reanalysis and numerical weather prediction models [*Mathias*, 2012; *Silva*, 2014; *de Abreu and da Rocha*, 2015]. The regular occurrence of SCs near densely populated and economically important regions of Brazil makes their study even more relevant.

SCs can happen in a wide variety of synoptic environments, with relatively cold mean sea surface temperature (SST) and strong vertical wind shear [*Evans and Guishard*, 2009]. Since SCs present some tropical characteristics, one would expect that it should develop over warm waters, but recent studies show that SCs can occur over a wide range of SST. *González-Alemán et al.* [2015] reported their occurrence over SST below 25°C in the eastern sector of North Atlantic basin. *Guishard et al.* [2009] pointed out subtropical cyclogenesis over SST near 15°C in the North Atlantic basin as a whole. *Evans and Braun* [2012], in their 50 year climatology of SCs over the South Atlantic, found that the median SST coincident with subtropical genesis is 18°C, while the median North Atlantic SST is 26°C. Composite analysis in the 33 year climatology by *Gozzo et al.* [2014] showed that during SC events the mean SST in South Atlantic does not exceed 25°C, and the surface latent and sensible heat fluxes are close to the climatological value.

Nevertheless, SCs in southwestern South Atlantic occurs where there is large moisture content in lower levels of the troposphere [*Dias Pinto et al.*, 2013; *Gozzo et al.*, 2014]. If local evaporation during these events is not

unusually intense, the transport of water vapor from distant regions by the atmospheric circulation should be a vital moisture source. Such remote transport has been reported in the case of tropical and extratropical cyclogenesis [e.g., *Lee*, 1989; *Silva et al.*, 2011] and should be a plausible mechanism to provide the necessary moisture source for southwestern South Atlantic SC under conditions of relatively cold SST.

A method for identifying remote moisture sources is the Lagrangian analysis, in which changes in the water vapor content of air parcels—due to evaporation and precipitation processes—are calculated along the trajectory of these parcels, from the source region up to the point of interest [*Sodemann et al.*, 2008]. This tool has been successfully applied to study the atmospheric branch of hydrological cycle in several regions around the planet [*Stohl and James*, 2004; *Nieto et al.*, 2006; *Drumond et al.*, 2008; *Gimeno et al.*, 2010; *Durán-Quesada et al.*, 2012; *Gimeno et al.*, 2013; *Drumond et al.*, 2014]. Concerning the study of cyclogenesis, the Lagrangian analysis has been mostly applied to identify the water vapor transport to and by extratropical cyclogenesis [*Bao et al.*, 2006; *Durán-Quesada et al.*, 2010; *Ordóñez et al.*, 2013; *Liberato et al.*, 2013]. Few studies using the Lagrangian viewpoint are currently available for SCs. One of the only works, by *Garde et al.* [2010] points that the air parcels present in the development of SC "the Duck," near the eastern coast of Australia, had its origin in remote tropical (extratropical) low levels (upper levels) of the troposphere, contributing to a hybrid structure of the system. The climatology of moisture transport associated with SCs was not addressed yet.

The aim of this work is to investigate the moisture sources associated with SC development over southwestern South Atlantic applying both Lagrangian analysis and numerical experiments with Weather Research and Forecasting (WRF) model. The Lagrangian technique, using the "Flexible Particle dispersion model" (Flexpart), was applied to the ERA-Interim reanalysis in the period of 1980–2015 and provided the main moisture sources to SCs. A numerical case study using the WRF model was carried out to assess the relative importance of local and remote moisture sources during SC development. This work is a complement of the results presented in *Gozzo et al.* [2014], bringing analysis for a slightly larger period and set of SCs.

2. Data and Methods

2.1. Data

The European Centre for Medium-Range Weather Forecasts, ERA-Interim reanalysis, hereafter ERA-Interim, described by *Dee et al.* [2011] was used in this work. From ERA-Interim, we used the variable horizontal wind, vertically integrated horizontal moisture flux, sea level pressure, geopotential height, and air temperature at every 6 h (0000, 0600, 1200, and 1800 UTC), with horizontal grid spacing of 1° of latitude by longitude and 61 vertical levels, from 1000 to 0.1 hPa.

2.2. Flexpart-Lagrangian Trajectories

Moisture sources for SCs were determined using the Lagrangian particle dispersion model Flexpart [*Stohl and James*, 2004; *Stohl et al.*, 2005], which computes changes in atmospheric moisture along trajectories. Flexpart model divides the atmosphere in a large number of three-dimensional finite elements called "particles" that are transported using the three-dimensional ERA-Interim wind data. The position (latitude and longitude) and specific humidity (q) are recorded at every 6 h. Increases due to evaporation (e) and decreases during precipitation (p) of the specific humidity are calculated through changes in (q) with time: $e - p = \mathrm{m}\, \mathrm{d}q/\mathrm{d}t$, where m is the mass of each particle. By adding e and p for all the particles in an atmospheric column over an area, we determine ($E - P$) fields, where E is the surface freshwater flux, or evaporation rate, and P is the precipitation rate, per unit area.

Flexpart model was used to find source regions for the atmospheric moisture present over the southeastern coast of Brazil (30.58–21.8°S and 49.58–35.58°W, hereafter RG1), during SC events. These events were selected by the criteria and tracking methods described in *Gozzo et al.* [2014], which have identified the RG1 as the region of western South Atlantic where most of the SCs have their genesis. In a period of 36 years (January 1980 to December 2015) a total set of 150 SCs was used to identify source regions of the moisture present in RG1 in subtropical cyclogenesis time (defined as 1200 UTC of the day when the cyclone was first identified by the tracking algorithm). In this analysis, only SCs first identified inside the RG1 were considered; i.e., the systems that developed outside RG1 and after entered the area were not considered.

The regions where air parcels gained moisture before reaching the RG1 were assessed integrating Flexpart backward in time. In the cyclogenesis time, the atmosphere was divided into approximately 2.0 million particles, with the next time steps showing the position of all particles in preceding times. In the previous positions, the model calculates the moisture balance for each particle and sums all particles to obtain the spatial distribution of $(E - P)$. The resulting $(E - P)$ distributions are composites for all subtropical cyclogenesis during the 36 year period in each austral season, being 83 events for summer (December-January-February), 37 events for autumn (March-April-May, MAM) and 30 events for spring (September-October-November); no SCs were found over RG1 in winter. The transport time was limited to 10 days, which is the average residence time of water vapor in the atmosphere [*Numaguti*, 1999; *Drumond et al.*, 2014].

2.3. Numerical Experiments

A numerical case study was carried out using the WRF-Advanced Research WRF version 3.5.1 model [*Skamarock et al.*, 2008]. This model solves the complete compressible and nonhydrostatic dynamic equations, discretized in the horizontal in an Arakawa C-grid and vertical coordinates following the terrain. The model domain spans 400 by 250 grid points, respectively, in east-west (70°W to 10°W) and north-south (37°S to 3°S) directions with horizontal grid spacing of 15 km and 37 vertical levels. A five grid-point buffer zone was specified along the boundaries, being the lateral boundary conditions given at every 6 h from the ERA-Interim reanalysis. This same data set was used as initial condition. The simulations used a time step of 80 s, starting at 0000 UTC on 25 February 1999 and ending at 0000 UTC on 8 March 1999, with the first 24 h discarded for model spin-up. The microphysics scheme used was the bulk Goddard scheme [*Tao et al.*, 1989], and the cumulus convection parameterization was the Betts-Miller-Janjic scheme [*Janjic*, 1994]. These parameterizations were selected after testing many model cofigurations, evidencing the importance of these processes to realistically simulate a SC event and the challenge to forecast such systems. The boundary layer parameterization was provided by the Yonsei University scheme [*Hong et al.*, 2006]. The surface layer parameterization, which directly computes the turbulent latent and sensible heat fluxes, uses the Similarity Theory [*Monin and Obhukov*, 1954] with a scheme proportional to the vertical thermal gradient to better calculations under weak wind conditions. A more detailed description of these parameterization schemes can be found in *Skamarock et al.* [2008].

3. Results

3.1. Lagrangian Analysis

The backward trajectories of Flexpart model show regions where the air parcels gained or lost moisture before reaching the RG1 area at the cyclogenesis time. In the resulting maps, regions with $(E - P) > 0$ are shown with warm colors and indicate that at that position and time the air parcels (that are bound to reach the RG1) are gaining moisture since evaporation is greater than precipitation. On the other hand, regions with $(E - P) < 0$ are shown with cold colors (blue) and indicate the regions where air parcels are losing moisture before reaching RG1. The $(E - P)$ field for day -1 represents the integrated mean moisture balance 1 day before all cyclogenesis events in the season, and the day -5 represents the mean for 5 days before all the SC events and so on.

For each season, Figure 1 presents only results from day -1, day -3, day -5, and day -7 prior to the cyclogenesis day. During austral summer, 1 day before the SCs, negative values of $(E - P)$ over the continent, in the western side of RG1, indicate that precipitation is larger than evaporation due to local convection (Figure 1a). In this area, convection is favored by high temperature during summer and enhanced by the northwesterly flow convergence at lower levels and negative geopotential anomalies at upper levels, which characterize the synoptic environment 1 day before cyclogenesis [*Gozzo et al.*, 2014]. Positive values to the south and east of the RG1 are associated with the local evaporation (that is, evaporation from the underlying ocean) increasing the atmospheric moisture. Three and 5 days before cyclogenesis, strong positive values of $(E - P)$ are a signal of moistening of the air parcels by evaporation over the ocean, in a broad area to the east and northeast of RG1 (Figures 1b and 1c). Over the ocean, the South Atlantic Subtropical High (SASH—centered approximately in 30°S–10°W) imposes a predominance of the evaporation over precipitation and the water vapor supplied to the atmosphere is transported toward the RG1 by the persistent northeasterly flow (as indicated in Figure 1a). Other source regions to the south and southeast of RG1 result from the air parcels advected by southerly winds associated with transient anticyclones displacing in higher latitudes (near

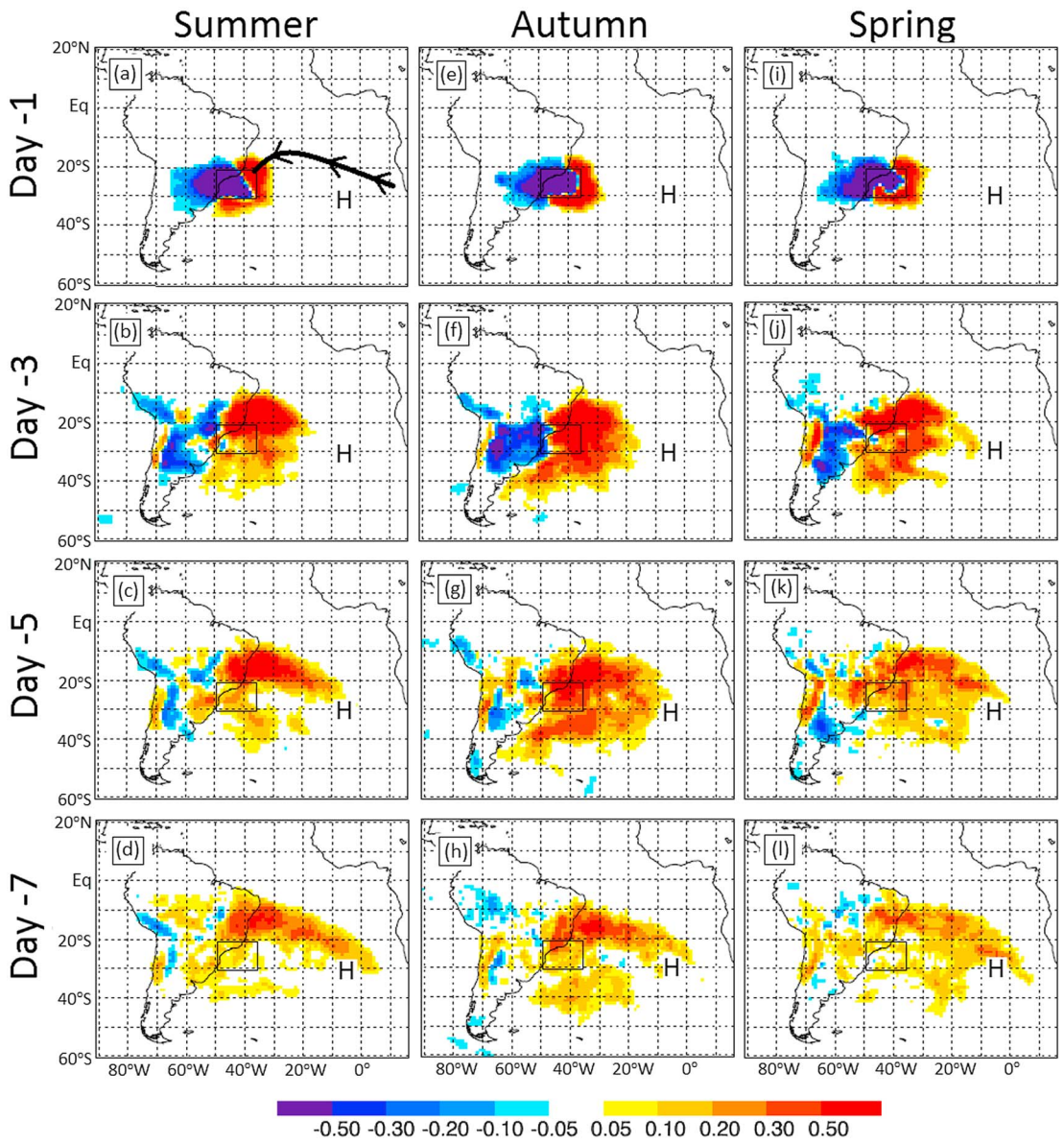

Figure 1. (a–d) Austral summer, (e–h) autumn, and (i–l) spring average ($E - P$) for −1, −3, −5, and −7 days before cyclogenesis. Units are in mm d^{-2}. The black box marks the position of RG1, where all the particles are bound to be at the time of cyclogenesis. Capital H indicates the approximate center of the South Atlantic Subtropical High in each season, and part of the circulation of the High is sketched in Figure 1a.

40°). Seven days before cyclogenesis, the strongest moisture source is located in the northern flank of the SASH (Figure 1d), with air parcels gaining moisture in far regions of the Atlantic and being later transported by the SASH flow into the RG1. Over the continent, on day −3, water vapor from evapotranspiration of the Amazon rainforest 7 and 5 days before cyclogenesis (Figures 1c and 1d) is converted to precipitation over Peru, Paraguay, and northern Argentina (Figure 1b).

The spatial pattern of ($E - P$) in Figures 1a–1d suggests the tropical sector of the South Atlantic Ocean, between 15°S and 10°S and extending from the southwestern African coast, as the main moisture source for the RG1 during subtropical cyclogenesis. *Drumond et al.* [2008] and *Drumond et al.* [2010] also identified this area as an intense moisture source region feeding precipitation over the La Plata basin and southwestern South Atlantic. However, these works also pointed out the equatorial Atlantic (north of Guyana—near 55°W–10°N) as an important source region to Central Brazil and southwestern South Atlantic, but the present results do not show significant contribution from this area to the RG1 during subtropical cyclogenesis.

The absence of this equatorial Atlantic moisture source (even when the backward analysis reaches 10 days—figures not shown) is an evidence that the South American Low-Level Jet (SALLJ) to the east of Andes Mountains is not an important mechanism to transport water vapor into the RG1 in subtropical cyclogenesis episodes. SALLJ is a poleward north-northwesterly wind maximum at low levels (between 800 and 700 hPa), centered near 60°W–20°S, that transports moist and warm air from the Amazon region toward the southeastern South America [*Vera et al.*, 2006]. In the present analysis, most of the water vapor originated in Amazon evapotranspiration precipitates over the continent, before reaching the RG1 (Figures 1a–1d). The negligible impact of SALLJ in RG1 is due to its climatological mean position that mainly promotes the moisture transport into Paraguay, northern Argentina, Uruguay, and southern Brazil [*Marengo et al.*, 2004]. *Durán-Quesada et al.* [2010] reinforces the present conclusions by comparing moisture sources for two extratropical cyclones, one formed near Uruguay and the other formed over RG1. In the former case, water vapor transported from the SALLJ was the main moisture source, while in the latter case evaporation came mostly from the ocean, near southeastern coast of Brazil.

Gozzo et al. [2014] discussed that the cyclogenesis region occurs in a confluence between northwesterly flow coming from the Amazon region and northeasterly SASH flow over the Brazilian coast. The Lagrangian analysis, showing the small impact of the SALLJ during SC episodes, suggests that the confluence is not associated to the low-level jet. Instead, the cyclonic circulation of a thermal low originated in the central part of South America and strengthened some days before subtropical cyclogenesis [*Gozzo et al.*, 2014] provides the northwesterly flow transporting water vapor from lower latitudes.

The $(E - P)$ field for autumn, in day -1 (Figure 1e), is similar to the summer, but the precipitation covers a slightly greater area over the RG1 and the evaporation region is more spread to the southeast and south of the box. Three days before cyclogenesis (Figure 1f), local evaporation and water vapor from the northeast and east of the RG1 are important moisture sources, but unlike the summer, moisture sources to the south of RG1 have the same magnitude. This pattern remains in day -5 (Figure 1g), and in day -7 the main moisture source lies to the north of SASH (Figure 1h). By comparing summer and autumn, the main differences are the greater contribution from local evaporation and the strongest source southward of RG1: the presence of a stronger transient high-pressure system and more intense surface heat and moisture fluxes during autumn, discussed in *Gozzo et al.* [2014], are the reasons for this difference.

The region to the south of RG1 is also an important moisture source during day -3 in spring (Figure 1j), but in the previous days, only the local evaporation and—again—northern sector of SASH are significant sources. The central regions of Brazil present the most intense contribution in spring, and the precipitation of this moisture only occurs in day -1, over the RG1, and not since day -5, as in summer.

Comparing $(E - P)$ fields in the three seasons, the moisture present in RG1 during subtropical cyclogenesis comes mainly from the northern flank of SASH. This agrees with results from *Herdies et al.* [2002] and *Drumond et al.* [2008], that also points this region as an important moisture source for La Plata basin, which is near to the RG1. Autumn is the season when the moisture sources are stronger and most widespread. This is a consequence of more intense near surface fluxes [*Gozzo et al.*, 2014] and may explain why the most intense and well-organized SCs occurred in this season (e.g., Catarina March 2004, Anita March 2010, Arani March 2011, and Cari March 2015).

SCs are not recurrent over the RG1, with a mean occurrence of only seven cyclones/year [*Gozzo et al.*, 2014]. It is reasonable to suggest, then, that the moisture sources depicted in Figure 1 are anomalous, transporting in these specific days an above-normal content of moisture to RG1. In order to analyze this, the source regions (that is, only where $E - P > 0$) 7 days before the 150 cases of cyclogenesis were compared to the seasonal mean source for each season in the period of 1980–2015. The results are the maps of moisture source anomaly, as mean for 7 days before cyclogenesis, shown in Figure 2.

For the three seasons, the anomalous field shows an increased moisture transport from the northeast of RG1 before SCs. In autumn (Figure 2b) there is also anomalous moisture source southward of RG1, due to transient high-pressure systems moving from west to east at high latitudes. In all seasons, a negative anomaly over the RG1 suggests that the surface local latent heat flux is weaker in the days prior to the subtropical cyclogenesis. This is an important result: the local turbulent moisture fluxes have below normal intensity at times preceding the formation of SCs that, at first, would depend strongly on low-level humidity to form and develop. Though the analysis covers only times before the cyclogenesis, it has been shown

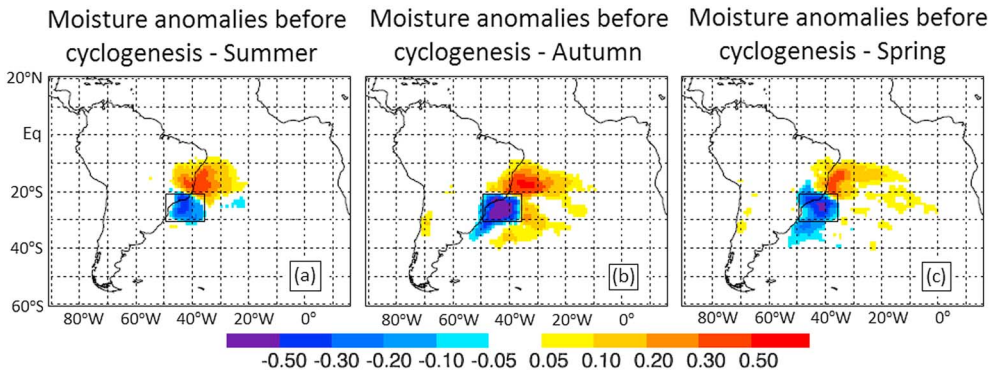

Figure 2. ($E - P$) anomalies (in mm d^{-2}) integrated for 7 days preceding subtropical cyclogenesis in austral (a) summer, (b) autumn, and (c) spring. The black box marks the position of RG1, where all the particles are bound to be at the time of cyclogenesis.

in *Gozzo et al.* [2014] that even 24 h after the cyclone is formed, the local surface heat fluxes are not much different from their climatological mean.

3.2. Eulerian Analysis

The Lagrangian analysis of moisture sources presented in section 3.1 gives a view of the moisture transport from distant regions toward the RG1 area. The Eulerian analysis, using the vertically integrated moisture fluxes, complements that information by linking the moisture variations to changes in the horizontal wind field.

From an Eulerian point of view, moisture source regions are characterized by moisture flux divergence [*Trenberth and Guillemot*, 1998]. Then, the northern and eastern sectors of the SASH are a significant climatological moisture source region during summer and autumn (Figures 3a–3d). *Gimeno et al.* [2010] identified the same source region persisting throughout the year and showed that the moisture originated there contributes to precipitation over the Atlantic branch of the Intertropical Convergence Zone, northern and eastern South America, central and western Africa, and, during austral summer, mainly over the southwestern South Atlantic (including the RG1). Figure 3a also displays a northwest-southeast oriented band of moisture flux convergence over Central Brazil extending to the South Atlantic, characteristic of the austral summer months.

Composite analysis for 7 days before subtropical cyclogenesis presents the pronounced moisture source region of South Atlantic essentially unaltered, but there is a strengthened moisture flux convergence over the RG1, mainly in the central and eastern sectors. This increased convergence is due to more intense north and northeasterly winds toward the RG1 between 20° and 15°S, and weaker southerly winds southward of RG1. These changes in the horizontal wind field occur because some days before the SCs, a thermal low displaces from the continent to the RG1 [*Gozzo et al.*, 2014], intensifying the low-pressure area that is a climatological characteristic of this region during summer [*Fernandez et al.*, 2006]. The enhanced cyclonic circulation is shown in the moisture flux anomaly field (Figure 3c). Bluish areas in this figure show increased moisture flux convergence occurring before SCs. The anomalous flux convergence over most of the RG1 could weaken the vertical humidity gradient between the ocean and the adjacent atmosphere, resulting in lower than average local turbulent fluxes (negative area inside RG1 in Figure 2a).

The climatology of autumn months (Figure 3d) shows again the low latitudes and the Atlantic near the African coast as important moisture sources. Another source region is seen along the coast of southeastern and south Brazil, including the RG1 and extending to higher latitudes, because of an increasing frequency of colder and drier air masses displacing from the continent toward the ocean that presents still warmer SST after summer [*Reboita et al.*, 2010]. This enhances turbulent fluxes of water vapor from the underlying ocean to the atmosphere, and the vapor then diverges from the region. However, in the days before SCs the situation over RG1 is reverse and the moisture flux convergence dominates over the southeastern coast of Brazil (Figure 3e). In the anomaly map (Figure 3f) there is a clear intensification of the northeasterly moisture transport toward the RG1 prior to SCs. In higher latitudes, a broad anticyclonic circulation anomaly (centered

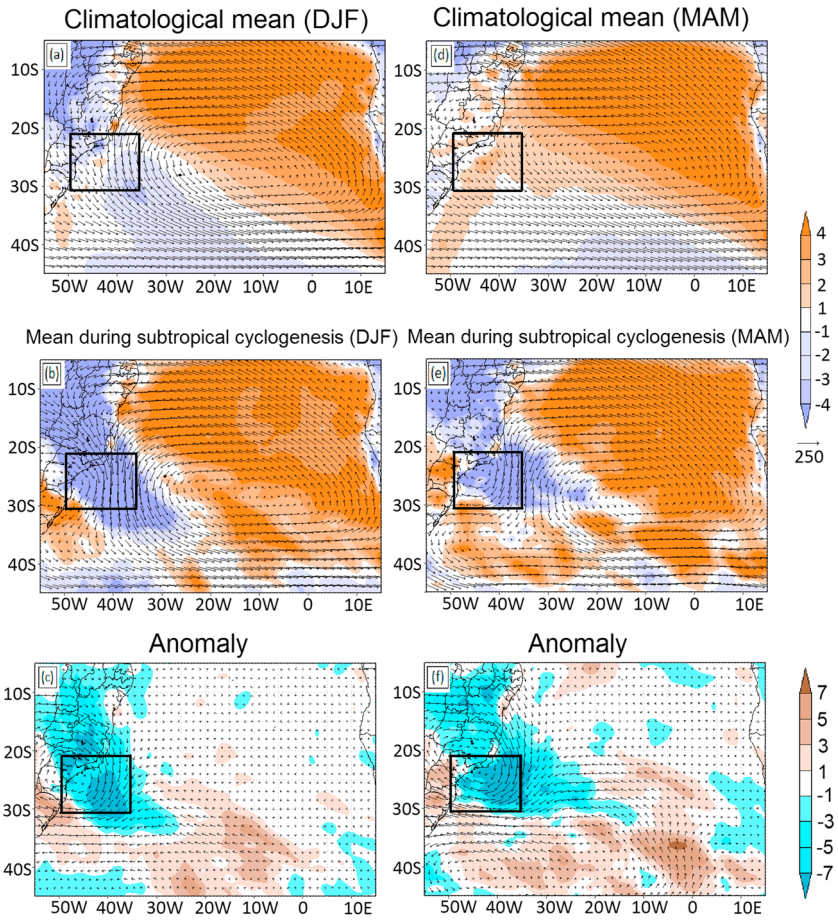

Figure 3. Vertically integrated horizontal moisture flux (vectors, in kg m^{-1} s^{-1}) and moisture flux divergence (shaded, in kg s^{-1}) for the period of 1980–2015: climatological mean in (a) summer and (d) autumn; composites for 7 days before cyclogenesis in (b) summer and (e) autumn, and anomalies for (c) summer and (f) autumn. The black box marks the position of RG1.

in 20°W–40°S) indicates the persistence of intense transient midlatitude anticyclones, weakening the northwesterly flow southward of RG1 (strong transient high-pressure areas occur along with autumn SCs in this region [*Gozzo et al.*, 2014]). The horizontal wind anomalies lead to stronger moisture flux convergence over RG1, with magnitude greater than in summer. Accordingly, the local moisture turbulent fluxes are also decreased (Figure 2b). The mean distribution of moisture flux convergence in the climatology and 7 days before cyclogenesis is similar in spring (figures not shown).

The strong moisture flux convergence evident 7 days before SCs suggests that the development of these systems may be more dependent to the moisture flux converging in the region prior to the genesis, than to the local turbulent fluxes during the cyclone development over the Brazilian coast. The dependence of prior moistening of the environment is verified in extratropical bomb cyclogenesis, which is weaker without the moistening [*Kuo et al.*, 1991; *Piva et al.*, 2011], and may be important in the case of SCs as well. An important difference, though, is the origin of the water vapor in each case: for the bomb cyclogenesis, it comes mainly from local latent heat fluxes inside the development region, while in the SCs under study it comes mainly from the convergence of water vapor flux brought from nonlocal sources.

In all three seasons analyzed, there are no significant changes in the magnitude of moisture flux divergence from the main sources (northern and eastern flanks of SASH). Then the evaporation in these regions is not different from the climatological mean before the cyclogenesis, and the anomalous convergent moisture flux is mostly associated with changes in the horizontal low-level wind field. A different situation occurs in the subtropical South Atlantic, especially during autumn: the anomalous flux divergence south and

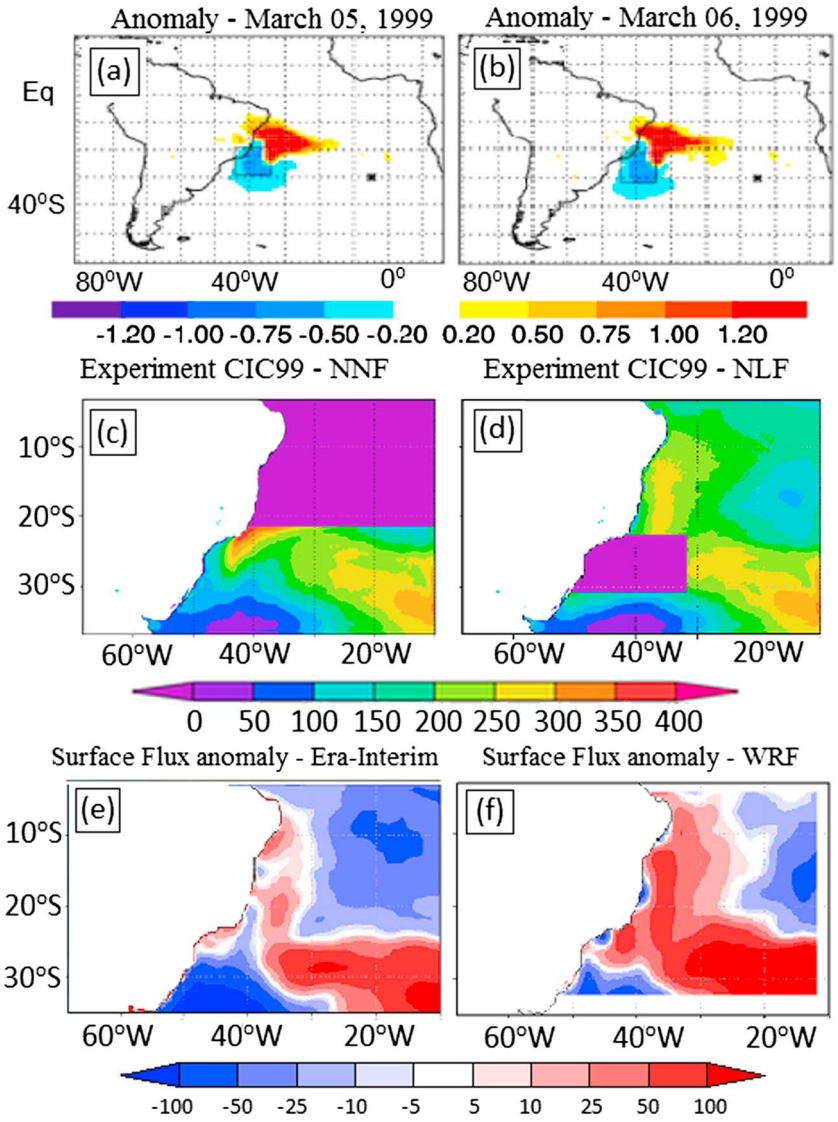

Figure 4. ($E - P$) anomaly from the MAM climatological mean, integrated 7 days before the analyzed day, for (a) 5 and (b) 6 March 1999. The box, centered in the coordinates of cyclone center at each time, marks the area where all the particles are located at 1200 UTC of the analyzed day. Simulation domain and location of the areas with zero latent heat flux (purple boxes) for (c) NNF and (d) NLF experiments, together with the mean (for the period of 3–8 March 1999) surface latent heat fluxes (shaded, in W m^{-2}) during CIC99. Surface latent heat flux (shaded, in W m^{-2}) anomaly (difference between CIC99 extended period, from 0000 UTC on 25 February until 0000 UTC on 8 March and the 1980–2015 MAM climatology), for (e) Era-Interim and (f) WRF CIC99-CTRL simulation.

southeastward of the RG1 suggests increased evaporation as transient anticyclones inhibit precipitation and cloudiness.

3.3. The Importance of Different Moisture Sources: Numerical Study

Gozzo et al. [2014] showed that the RG1 subtropical cyclones develop in a moist environment though they occur over relatively cold SSTs and turbulent latent heat fluxes near or below the climatological values. As presented in previous sections, in the days before the SC development anomalous amounts of water vapor were advected from the South Atlantic low latitudes toward RG1 by the SASH flow, suggesting that SCs have strong dependence of the nonlocal atmospheric moisture sources located northeastward. When upper level cold disturbances (cutoff lows in 500 hPa) move over the warm and moist layer formed by this advection, strong convection is triggered helping to sustain SCs.

The relative importance of local and nonlocal moisture fluxes is evaluated by means of a numerical case study. The cyclone under study formed on 4 March 1999, and is a subtropical system following the criteria of *Gozzo et al.* [2014]. It was characterized as a "pure" SC, i.e., does not show any transition process. The Cyclone Phase Space (CPS) analysis [*Hart*, 2003] for this cyclone shows that it presented small values of the parameter B and positive (negative) values of $-V_L^T$ ($-V_U^T$), placing it in the "symmetric shallow warm-core" region of the CPS phase diagram during all its lifetime (Figures 6e and 6f). The choice of this particular system, hereafter CIC99, is also based in its Lagrangian moisture source analysis. In the period of 4–7 March, $(E - P)$ anomalies compared to the climatology (mean of March-April-May) were calculated for a mobile box of 10° × 10° of latitude by longitude following the center of the cyclone. The anomalies are again a mean of the 7 days prior to the analyzed day. In the anomaly fields (Figures 4a and 4b) a significant nonlocal moisture source is located northeastward of the cyclone center, and the development region (inside the small box) presents mean or slightly below mean $(E - P)$ values. This pattern is maintained from 3 to 8 March and suggests that the development of this cyclone may depend on the nonlocal moisture sources.

WRF model is used to simulate the development of CIC99 in a control experiment (CIC99-CTRL), which is compared to two sensitivity experiments: the first (CIC99-NNF—"no nonlocal fluxes") aims to confirm if the nonlocal moisture flux is necessary for the development of CIC99; the second experiment, named CIC99-NLF ("no local fluxes"), would determine whether this cyclone could develop without the contribution from local evaporation. Figures 4c and 4d show the full simulation domain, and where the surface latent heat flux was set to zero in each experiment, along with the distribution of oceanic surface latent flux over the Atlantic Ocean. In order to study the moisture sources before cyclone initial phase, analysis started 7 days before the genesis day; i.e., they cover the period from 25 February 1999 to 9 March 1999.

Figures 4e and 4f show the latent heat flux anomalies during the cyclone event (25 February to 8 March 1999). The anomalies are departures from the climatology for MAM of ERA-Interim in the period of 1980–2015. Positive values indicate regions where the latent heat flux was more intense during the event, while negative values show areas where the flux was weaker than the climatology during the analyzed days. These anomalies were well simulated by the CIC99-CTRL that shows less intense fluxes during the cyclone event over the northeastern flank of the SASH (near 20°W–10°S) and stronger than average fluxes to the northeast of the cyclone, along the Brazilian coast (near 35°W, from 25°S to 10°S). The positive anomaly to the northeast of the area where the cyclone will develop is consistent with the pattern of anomalous moisture transport presented in Figure 2a.

3.3.1. CIC99: Synoptic Evolution

According to the ERA-Interim reanalysis, CIC99 was first identified as low-pressure system located near 20°S–40°W at 0000 UTC on 4 March 1999 (Figure 5a). The cyclone presented closed isobars in the sea level pressure field 24 h later, with minimum pressure of 1008 hPa, lying under the axis of an elongated trough in 500 hPa (Figure 5b). In the next 2 days, the surface low remains quasi-stationary (near 27°S–40°W) and a cutoff low developed at 500 hPa (Figures 5c and 5d). The genesis of this cyclone follows the mechanism proposed by *Guishard et al.* [2009] and *Evans and Braun* [2012] for subtropical systems in the North Atlantic: a cold cutoff low in upper levels of the atmosphere induces vertical upward motions and intensifies a preexistent surface low. Composite analyses in *Gozzo et al.* [2014] show that most of the summer and autumn SCs in RG1 have developed in similar way.

At 0000 UTC on 4 March, low-level warm air advection by the northeasterly winds is contributing to the low-pressure area development near 20°S–40°W (Figure 5e). From 5 to 7 March at 0000 UTC, the warm air advection southeastward/eastward of the cyclone strengthen the midlevel ridge, and the cold air advection near 50°W deepens the upper cold-core low (Figures 5f–5h). The horizontal temperature advection pattern at these times is conducive to the formation of a cutoff low at 500 hPa [*Campetella and Possia*, 2007; *Godoy et al.*, 2011].

During the genesis and development of CIC99, strong low-level moisture flux convergence occurs in the cyclone area (Figures 5i–5l). Infrared satellite images from 4 to 7 March (Figures 6a–6d) show that the most intense convection is displaced eastward from the low-level circulation center, where the moisture flux and its divergence are maximum. At 0000 UTC on 6 March (Figure 6c) there is a signal of disorganized convection occurring poleward of the cyclone center, with the cloud pattern around the center starting to resemble an inverted comma-shape. On the next day (Figure 6d) this poleward convection is slightly

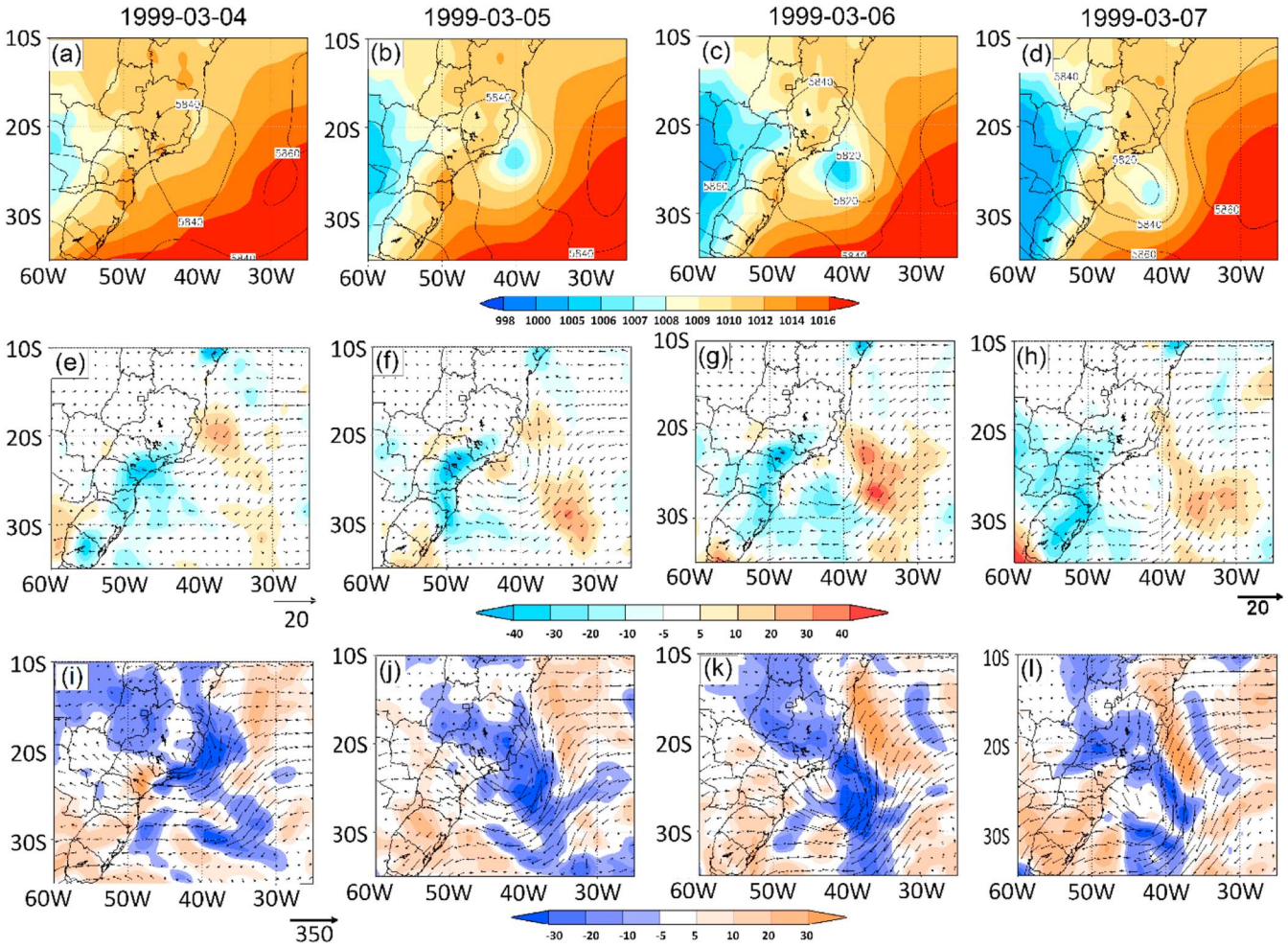

Figure 5. Synoptic evolution of CIC99 in ERA-Interim reanalysis: (a–d) Sea level pressure (shaded, in hPa) and geopotential height (contours, in m); (e–h) 850 hPa horizontal temperature advection (shaded, in K d^{-1}) and horizontal wind (vectors, in m s^{-1}). (i–l) Vertically integrated moisture flux (vectors, in kg m^{-1} s^{-1}) and its divergence (shaded, in kg s^{-1}). The fields correspond to 0000 UTC on 4 March 1999 (Figures 5a, 5e, and 5i) and 0000 UTC on 5 March 1999 (Figures 5b, 5f, and 5j), 6 March 1999 (Figures 5c, 5g, and 5k), and 7 March 1999 (Figures 5d, 5h, and 5l).

stronger, but the eastward convection decreases. Moisture flux divergence over the South Atlantic Ocean, to the northeast of the cyclone, characterizes the region as an important moisture source. This Eulerian viewpoint complements the Lagrangian maps of Figures 4a–4b.

3.3.2. CIC99-CTRL Simulation

The CTRL run shows the main features observed in ERA-Interim during CIC99 development: the initial formation near the southeast Brazilian coast, its quasi-stationary characteristic at low levels, and the formation of a cold cutoff low at 500 hPa (Figures 7a–7d). Nevertheless, the simulated surface low forms further south compared with ERA-Interim, and it moves to the northwest in the last 2 days (5 and 6 March). In addition, the simulated cyclone is more intense than in the ERA-Interim reanalysis, reaching a minimum pressure of 1002 hPa.

Despite the difference in the location of the CIC99, the spatial pattern of warm (cold) air advection to the east (west) of the surface low has large agreement with ERA-Interim, though the magnitude of this advection is somewhat overestimated compared to ERA-Interim (Figures 7e–7h). In these figures, the vector field corresponds to the vertically integrated horizontal moisture flux and shows the water vapor transport from low latitudes toward the region of the cyclone.

A distinctive feature of the SCs is the hybrid thermal structure, with warm air anomaly at low levels and cold air anomaly in upper levels [*Hart*, 2003; *Guishard et al.*, 2009, *Gozzo et al.*, 2014]. This thermal structure is

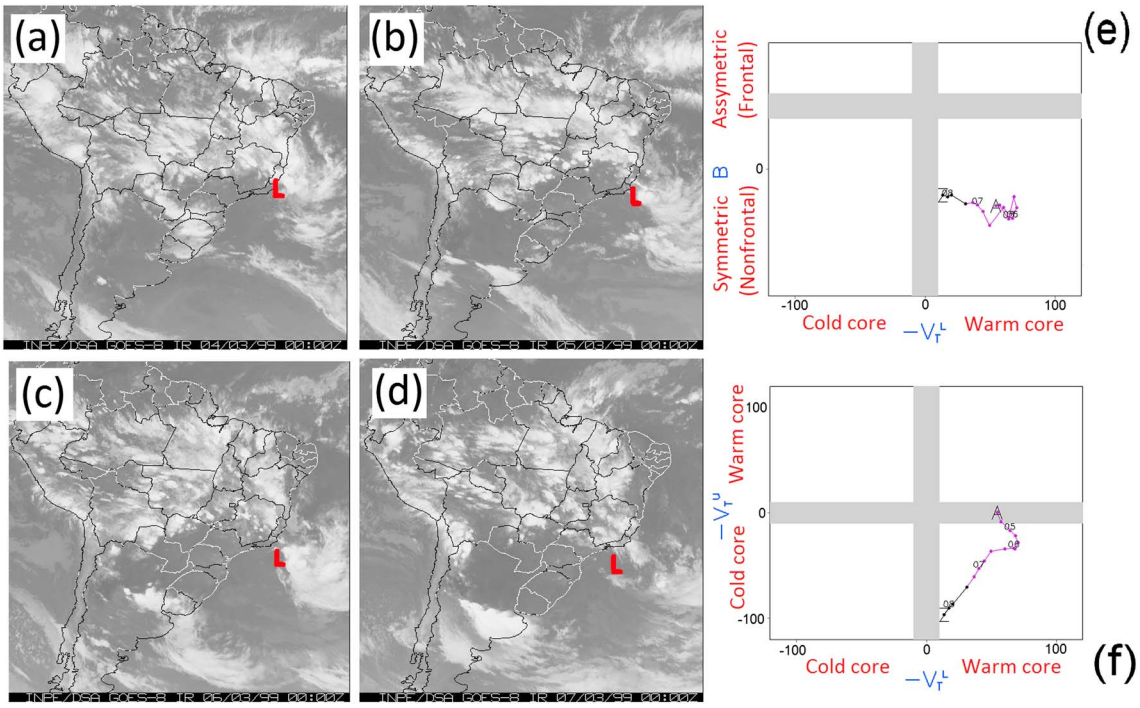

Figure 6. GOES 8 infrared images at 0000UTC for (a) 4, (b) 5, (c) 6, and (d) 7 March 1999. The red capital L indicates the approximate position of the low-pressure center according to the tracking algorithm. Cyclone phase diagram for the system from 1200 UTC on 4 March 1999 and 1200 UTC on 8 March 1999: (e) *B* versus $-|V_T^L|$ (f) $-|V_T^U|$ versus $-|V_T^L|$. Geopotential height, horizontal wind, and sea level pressure data used to construct the diagram are from the Era-Interim reanalysis.

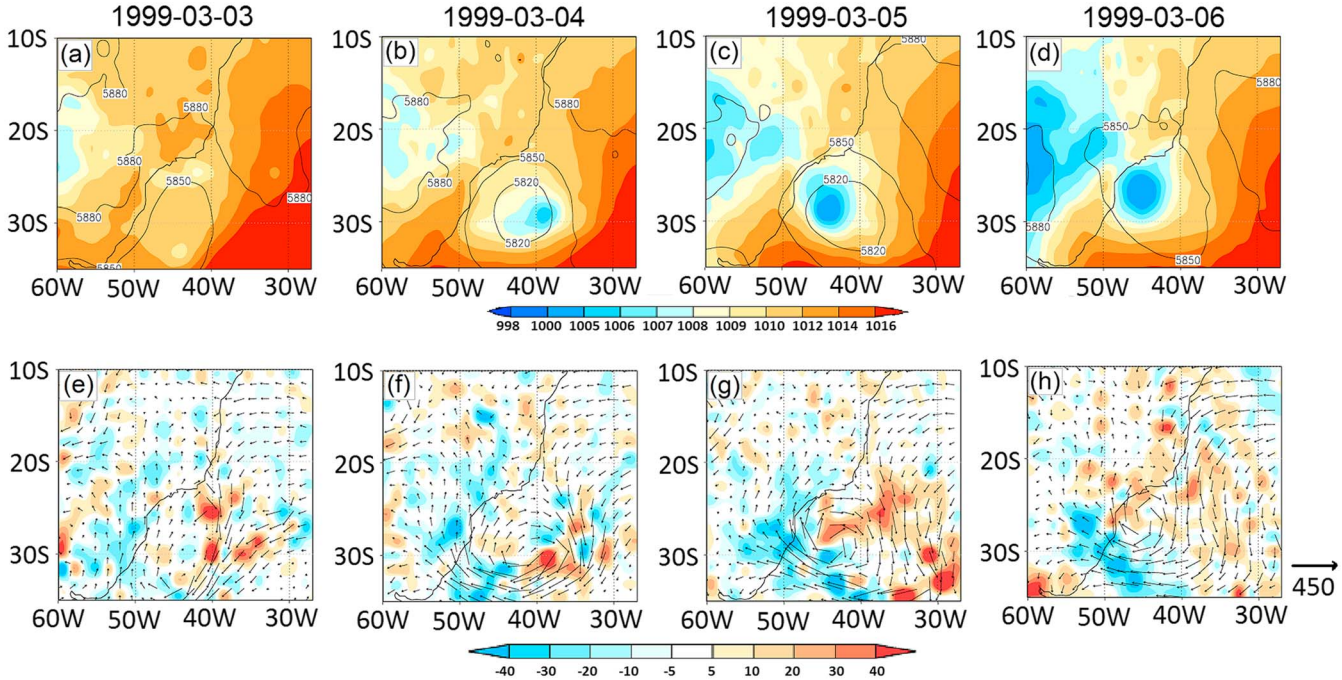

Figure 7. Synoptic evolution of CIC99-CTRL. (a–d) Sea level pressure (shaded, in hPa) and geopotential height (contours, in m); (e–h) horizontal temperature advection (shaded, in K d^{-1}) and vertically integrated moisture flux (vectors, in kg m^{-1} s^{-1}). The fields correspond to 0000 UTC on 3 March 1999 (Figures 7a–7e), 0000 UTC on 4 March 1999 Figures 7b–7f, 0000 UTC on 5 March 1999 (Figures 7c–7g), and 0000 UTC on 6 March 1999 (Figures 7d–7h).

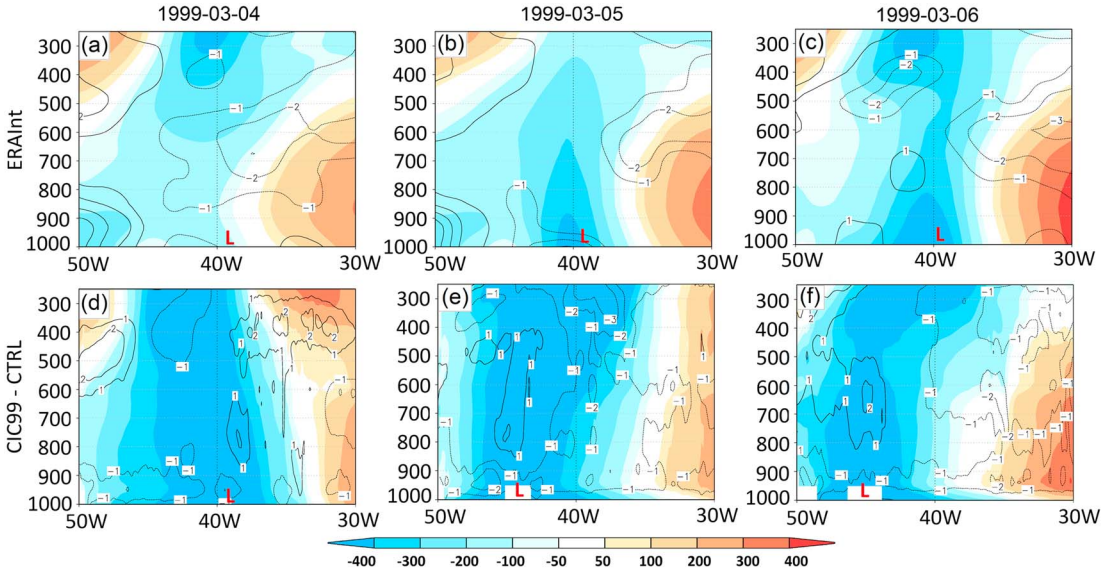

Figure 8. Vertical cross section, centered in the latitude of the cyclone center at each day, of air temperature (contours, in K) and geopotential height (shaded, in m) anomalies from the zonal mean, for (a–c) ERA-Interim reanalysis and (d–f) CIC99-CTRL. The fields correspond to 0000 UTC on 4 March 1999 (Figures 8a–8d), 5 March 1999 (Figures 8b–8e), and 6 March 1999 (Figures 8c–8f). The red capital L represents the position of the surface low.

evident in the ERA-Interim reanalysis from 0000 UTC on 6 March (Figure 8c), and it remains, with similar magnitude, at 0000 UTC on 7 March and 08 (figures not shown). In CIC99-CTRL there is the development of a low-level warm core, between 900 and 700 hPa, and an upper level cold core, between 500 and 300 hPa (associated with the cutoff low), since 0000 UTC on 4 March (Figure 8d). The simulated warm core intensifies during the next days, reaching an anomaly of +2 K in 650 hPa at 0000 UTC on 6 March (Figures 8e and 8f). In the geopotential anomaly field the system has a barotropic structure in both ERA-Interim and simulation, though the simulated cyclone develops approximately 5° eastward of that in the reanalysis.

3.3.3. Experiment CIC99-NNF

Experiment CIC99-NNF shows that the removal of nonlocal surface moisture fluxes prevents the development of the cyclone at the southwestern coast of Brazil (Figures 9a–9d). At 0000 UTC on 3 March, there was an incipient low pressure near 27°S–48°W, but it quickly disappeared. The cold cutoff low does not evolve in 500 hPa, reducing the convective potential in the troposphere. The absence of the cutoff low is a consequence of changes in the horizontal temperature advection pattern (Figures 9e–9h): the warm advection (near 40°W) is weaker than in CIC99-CTRL, due to the weaker northerly/northeasterly flow. The weaker flow occurs because the surface low and its associated pressure gradient do not form around 30°S–40°W. A cyclonic circulation does not develop, and the cold horizontal advection over the southern Brazilian coast is also weakened. These changes inhibit the deepening of the midlevel trough and later detaching of the cutoff low. In Figures 8e–8h, it is also evident the decrease of water vapor transport from northeast to the cyclone area.

The vertical profile of geopotential height crossing the center of CIC99-NNF (Figures 10a–10d) presents negative anomalies around 40°W, but with weaker intensity than seen in CIC99-CTRL. Besides, in NNF the warm core does not develop in lower levels: the temperature anomaly is either zero or cold (−1 K) from the surface to the upper levels. According to *Guishard et al.* [2009] and *Evans and Braun* [2012] the convection that leads to a warmer layer in the lower troposphere in SCs is modulated either by development over warm SST or horizontal warm air advection. In this experiment, SST and local surface fluxes over the cyclone are similar to the control simulation, so the changing in horizontal temperature advection by the absence of nonlocal fluxes may be playing a role in weakening the diabatic heating. Figures 10e–10h present the vertical profiles of horizontal temperature advection and the diabatic term of the thermodynamic equation, calculated over an area of 10° × 10° of latitude and longitude, centered in the center of the cyclone, for the CTRL and NNF simulations.

Warm advection occurs below 850 hPa at 0000 UTC on 3 and 4 March in the control simulation, as warmer air is being brought by the northeasterly flow from lower latitudes toward the region where the cyclone is

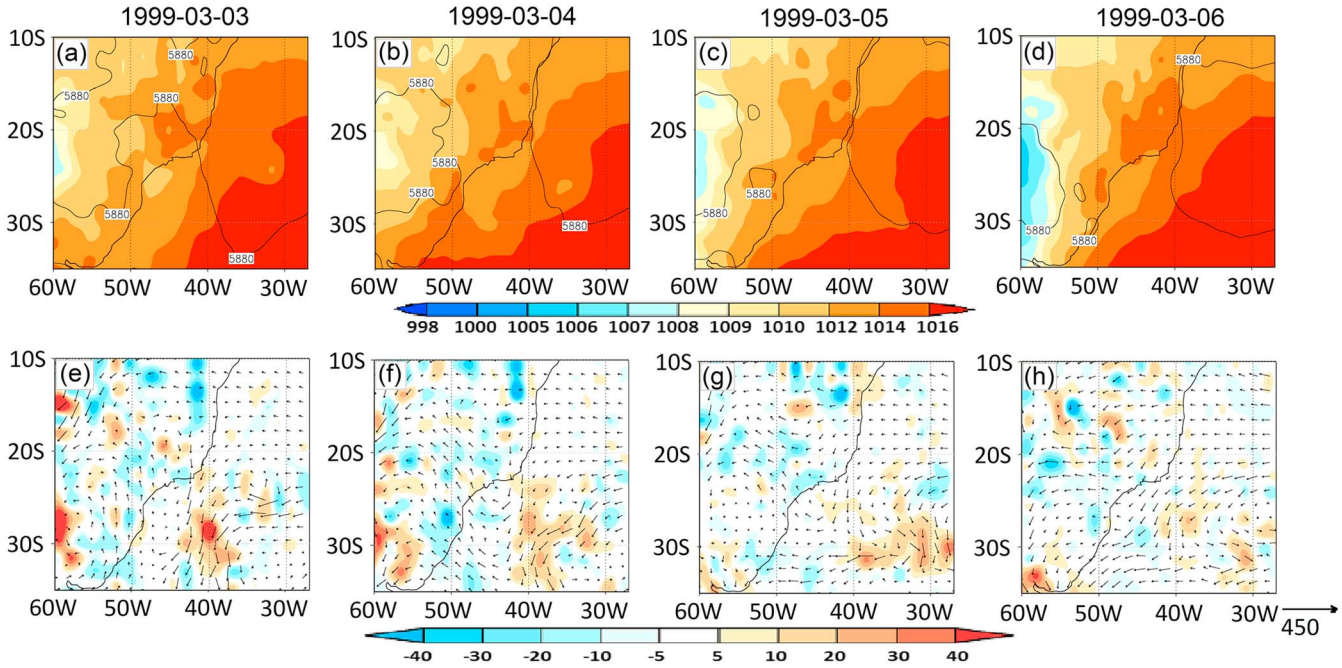

Figure 9. Synoptic evolution of CIC99-NNF. (a–d) Sea level pressure (shaded, in hPa) and geopotential height (contours, in m); (e–h) horizontal temperature advection (shaded, in K d^{-1}) and vertically integrated moisture flux (vectors, in kg m^{-1} s^{-1}). The fields correspond to Figures 9a–9e 0000 UTC on 3 March 1999, 0000 UTC on 4 March 1999 (Figures 9b–9f), 0000 UTC on March 1999 (Figures 9c–9g), and 0000 UTC on 6 March 1999 (Figures 9d–9h).

bound to develop (Figures 10e and 10f). The diabatic term is mainly negative during both days (due to radiative cooling, as the cloudiness associated with the cyclone only develops from the later hours of 4 March in CIC99-CTRL—figures not shown). CIC99-NNF also shows diabatic cooling predominating in both days, but unlike the control simulation, there is cold or no significant temperature advection below 700 hPa. Therefore, the formation of a warm-core low in this case is a result of warm air advection in the lower troposphere. This low-level heating enhances the vertical instability and induces cyclonic circulation

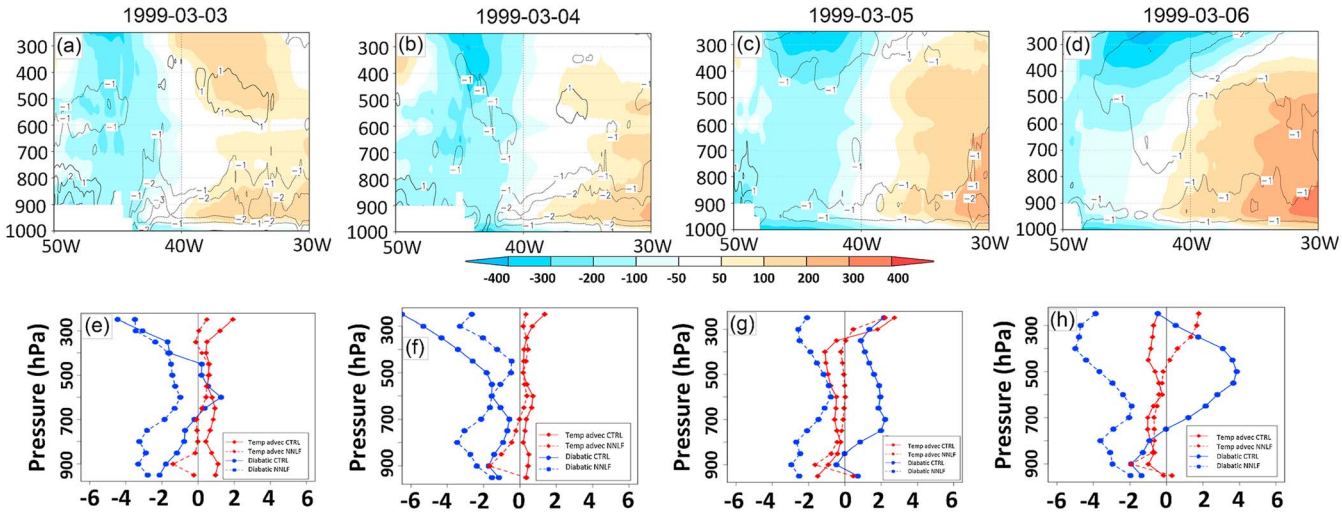

Figure 10. (a–d) Vertical cross section, centered in the latitude of the cyclone center at each day, of air temperature (contours, in K) and geopotential height (shaded, in m) anomalies from the zonal mean, in CIC99-NNF and (e–h) vertical profile of horizontal temperature advection (red lines) and diabatic heating (blue lines) around the cyclone center (in K day^{-1}) for the experiments CIC99-CTRL and CIC99-NNF. The fields correspond to 0000 UTC on 3 March 1999 (Figures 10a–10e), 0000 UTC on 4 March 1999 (Figures 10b–10f), 0000 UTC on 5 March 1999 (Figures 10c–10g), and 0000 UTC on 6 March 1999 (Figures 10d–10h).

near the surface, leading to cyclone development and cloud formation. In the absence of this forcing, and with less moisture in the lower troposphere (due to the reduced moisture transport from lower latitudes), the vertical profile of diabatic heating in CIC99-NNF remains negative during 5 March, while the convective activity in CIC99-CTRL produces a positive diabatic profile with maximum of +2 K d^{-1} near 700 hPa (Figure 10g). This diabatic heating increases the positive temperature anomaly at low levels (Figure 8e) contributing to maintain the warm core. In the present phase of cyclogenesis, cold air advection predominates from the surface up to 400 hPa. At 0000 UTC on 6 March, the diabatic heating associated to convection reaches its maximum value in CTRL simulation (+4 K d^{-1}, near 500 hPa), while the horizontal advection is negative throughout the troposphere (Figure 10h). In the NNF experiment, the diabatic term remains negative and cold air advection occurs between the surface and 500 hPa.

Figures 9e–9h show that CIC99-NNF produced a weaker cyclonic circulation with decreased northern warm air advection and mass convergence to the cyclone region, and Figures 10e–10h present the relative importance of this process and the moisture transport to the development of the SC. During all the experiment, changes in the diabatic term are larger than the changes in the air advection term, indicating that the moisture transport toward the SC region is more affected by the absence of nonlocal fluxes than the warm air advection. It indicates that the low-level moisture content is the man factor controlling the development of this SC, supporting our early hypothesis, and the mass convergence and warm air advection are a secondary process.

The absence of cyclone development when the nonlocal fluxes are completely removed is an important indicative of the role of these fluxes for subtropical cyclogenesis in South Atlantic. Therefore, an additional numerical experiment was conducted to reinforce these results. A simulation called CIC99-CLIM was carried out imposing the ERA-Interim MAM climatology (1980–2015) of the latent heat flux over the Atlantic Ocean. By using the climatological field, the anomalous latent heat flux (and consequently a significant part of the moisture transport) from the northeast was removed, and then a weaker SC would be expected to develop in CIC99-CLIM. Indeed, the CIC99-CLIM attained a minimum sea level pressure 3 hPa greater than in CIC99-CTRL (figures not shown). This simulation also supports the conclusion that a nonlocal latent heat flux anomaly located to the northeast of cyclogenesis area may help SC development, as indicated in Figure 2.

3.3.4. Experiment CIC99-NLF

In the absence of local surface moisture fluxes, the trough in 500 hPa (Figure 11a) still originates a cutoff low at 0000 UTC on 4 March (Figure 11b). At 0000 UTC on 3 and 4 March, the transport of water vapor by northeasterly winds and the horizontal temperature advection pattern are similar to the control simulation (Figures 11d and 11e). This synoptic situation leads to a closed surface low, with central pressure of 1010 hPa, located eastward of the midlevel cutoff low at 0000 UTC on 5 March (Figure 11c), and a temperature advection field similar to CIC99-CTRL. At 0000 UTC on 6 March, it is not possible to identify the cyclone in sea level pressure field anymore (figure not shown). The presence of nonlocal moisture is likely more important to the cyclone genesis, but its weaker intensity and quicker dissipation in CIC99-NLF indicate that surface local fluxes were important to the deepening and longer duration of the low after its formation, as also occurs for bomb and regular extratropical cyclogenesis over southwestern South Atlantic [*Piva et al.*, 2011; *Reboita et al.*, 2012; *Gozzo and da Rocha*, 2013].

In the vertical cross section of geopotential height in Figure 12, CIC99-NLF shows a stronger negative anomaly than NNF, since in the former case the closed cold low is formed in 500 hPa. In addition, as in ERA-Interim and CTRL, the system has a barotropic structure. However, the vertical profile of air temperature anomaly does not show a warm core at lower levels of the troposphere (Figures 12a–12c), preventing its classification as a SC.

Warm air advection occurs during the first day of development of CIC99-NLF, but it is less intense than in CTRL because the northeasterly flow is weaker (Figure 12d). At 0000 UTC on 4 March, the net temperature advection in the cyclone region is negative, as it was in NNF, but slightly weaker. This is due to a stronger warm air advection occurring at the eastern side of the low. The diabatic heating term is again negative (Figure 12e). On 5 March, the net temperature advection is positive from the surface up to 400 hPa, resulting from a cold air advection weaker than in CTRL. The diabatic heating term remains negative in all levels of the troposphere, and it has smaller magnitude than in NNF. The smaller intensity of diabatic cooling in NLF compared to NNF would be due to the greater amount of water vapor in the atmospheric column.

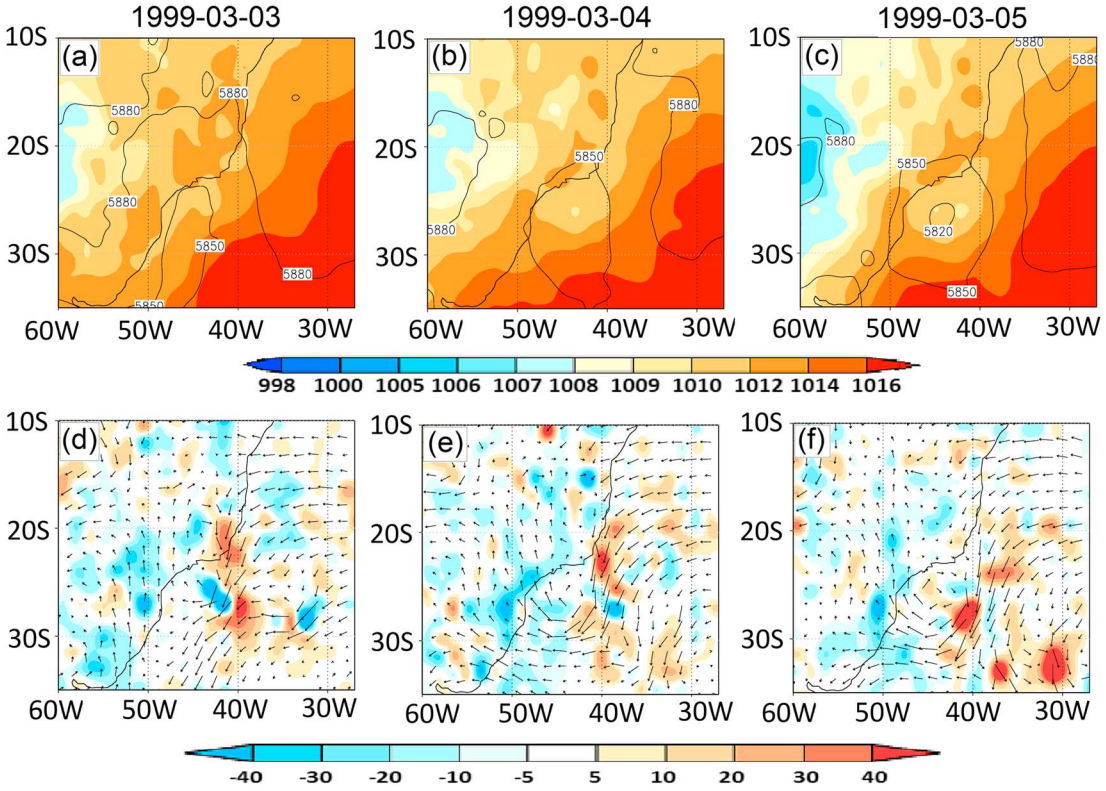

Figure 11. Synoptic evolution of CIC99-NLF. (a–c) Sea level pressure (shaded, in hPa) and geopotential height (contours, in m); (d–f) horizontal temperature advection (shaded, in K d^{-1}) and vertically integrated moisture flux (vectors, in kg m^{-1} s^{-1}). The fields correspond to 0000 UTC on 3 March 1999 (Figures 11a and 11d), 0000 UTC on 4 March 1999 (Figures 11b and 11e), and 0000 UTC on 5 March 1999 (Figures 11c and 11f).

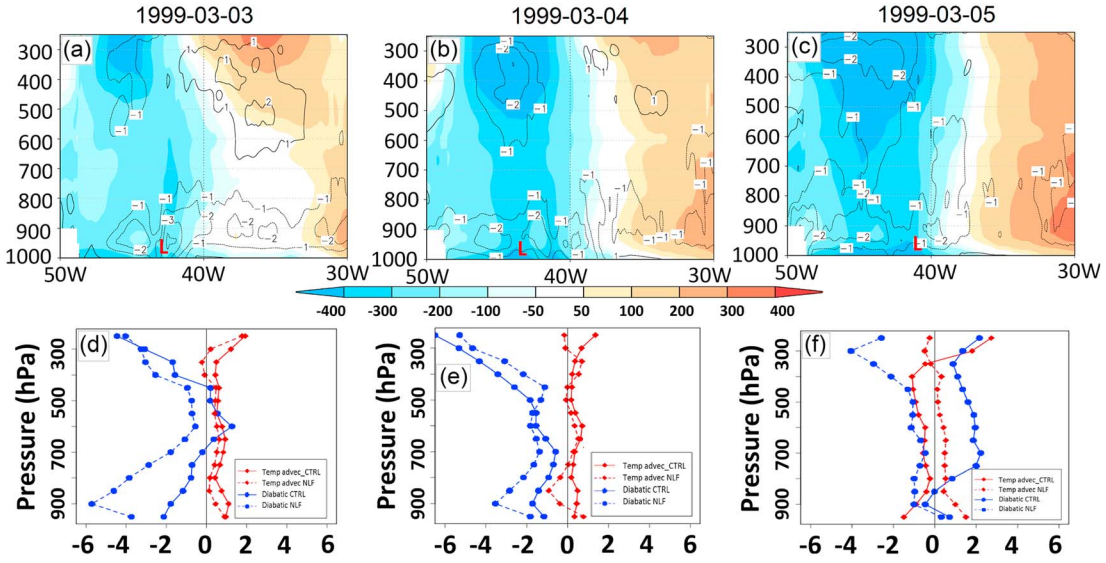

Figure 12. (a–c) Vertical cross section, centered in the latitude of the cyclone center at each day, of air temperature (contours, in K) and geopotential height (shaded, in m) anomalies from the zonal mean, in CIC99-NLF and (d–f) vertical profile of horizontal temperature advection (red lines) and diabatic heating (blue lines) around the cyclone center (in K d^{-1}) for the experiments CIC99-CTRL and CIC99-NLF. The fields correspond to 0000 UTC on 3 March 1999 (Figures 12a–12d), 0000 UTC on 4 March 1999, 0000 UTC on 5 March 1999 (Figures 12c–12f), and 0000 UTC on 6 March 1999 (Figures 12d–12g). The red capital L represents the position of the surface low.

The two experiments suggest that the combined effects of nonlocal and local moisture sources help to trigger the development of this subtropical cyclone as represented by the ERA-Interim reanalysis.

4. Summary and Conclusions

An analysis of moisture sources related to the development of subtropical cyclogenesis (SC) over the southwestern Atlantic Ocean (RG1) was presented using an objective Lagrangian trajectory model and numerical experiments.

Lagrangian trajectory analysis shows that most of the water vapor arriving in the RG1 during SC events originates in the South Atlantic Ocean to the northeast of the cyclogenesis region. The source region, located between 15°S and 10°S and extending almost to the western coast of Africa, has the largest evaporation rates in South Atlantic basin. In the days before SCs, there is anomalous transport of water vapor toward RG1 due to an intensification of northerly/northeasterly winds. The anomalous moisture transport to RG1 is favored during the austral summer months, when the western sector of the SASH is located near the Brazilian coast. During austral winter, the moisture transport parallel to the coast is weakened [*Trenberth et al.*, 2011] and no SC happened over the RG1 (although they have occurred over other sectors of South Atlantic [*Gozzo et al.*, 2014]). To the south of RG1, near the latitude of 30°S, there is another moisture source, resulting from mobile high-latitude anticyclones that increase surface latent heat fluxes and atmospheric moisture transported by the southerly winds toward RG1. This source is especially important for SCs during austral autumn, when more intense anticyclones are crossing southward RG1 [*Gozzo et al.*, 2014].

According to Lagrangian analysis, SALLJ has little contribution to the moisture transport toward RG1 during SCs. The tropical Atlantic does not appear as a moisture source, and the moisture from evapotranspiration over Amazon rainforest precipitates over the continent, a couple of days before SCs in RG1.

The occurrence of SCs over relatively cold SSTs in RG1 [*Gozzo et al.*, 2014] suggested that the nonlocal moisture source in low latitudes (between 15 and 10°S) of equatorial South Atlantic Ocean can be fundamental to the SCs formation. In order to assess the importance of the remote moisture source relative to the local evaporation, in the days preceding a case of SC, two numerical experiments were carried out using the WRF model. Turbulent latent heat fluxes were suppressed in the low latitudes of South Atlantic (first experiment) and over the area of SCs (second experiment).

In the first experiment, the SC did not develop. The absence of nonlocal moisture fluxes reduced the horizontal warm air advection toward the RG1 since the northeasterly flow parallel to the Brazilian coast was not established. Without the remote surface latent heat fluxes, the diabatic heating term remained negative and did not contribute to atmospheric instability during the times where the SC would develop. Both the low-level warm core and the midlevel cold cutoff low did not form because of weaker horizontal temperature advection. An additional simulation with diminished nonlocal latent heat fluxes developed a weaker SC, confirming and complementing the results of the nonlocal experiment. This simulation reinforced the importance of a northeastern surface flux anomaly to the development of the cyclone. This anomaly appears as an important feature that a forecaster could observe when assessing whether a SC is likely to form near the southeastern Brazilian coast.

Results from the second experiment show that in the absence of local evaporation a weaker and short-lived cyclone formed. At midlevels, the cold cutoff low was present, but the atmospheric column instability was weaker due to a drier environment and slower upward motions. Less moisture and weaker upward motions reduced the convective activity, and the SC region experienced diabatic cooling, damping the system development. It is important to notice that even though there was a cyclone development in the absence of a local moisture source, it did not present subtropical characteristics. Instead, it presented a pure cold core, as an extratropical system. Therefore, the combined effect of local and nonlocal moisture sources seemed to allow the formation of this SC event.

Given the climatological results, both the low latitudes and local moisture sources may be necessary for SC development over the RG1. The application of the present methodology to perform sensitivity experiments in a climatological scale is suggested to complement the present results.

Acknowledgments
Luiz Felippe Gozzo would like to thank the Ciencia sem Fronteiras project, grant 238765/2012-1, from the Conselho Nacional de Desenvolvimento Cientifico e Tecnologico (CNPq). This work was supported by CAPES/PROEX and the CNPq grants 558121/2009-8, 307202/2011-9, 140839/2011-9, 481942/2013-0, and FAPESP grant 2008/58101-9. The data used here are available for scientific purposes by the European Centre for Medium-Range Weather Forecasts following registration (http://apps.ecmwf.int/datasets/data/interim-full-daily/levtype=sfc/). The source code for the Flexpart model is available at https://www.flexpart.eu/. The authors would like to thank the anonymous reviewers for their helpful suggestions and comments on an earlier version of this manuscript.

References

Bao, J.-W., S. A. Michelson, P. J. Neiman, F. M. Ralph, and J. M. Wilczak (2006), Interpretation of enhanced integrated water vapor bands associated with extratropical cyclones: Their formation and connection to tropical moisture, *Mon. Weather Rev.*, *134*, 1063–1080.

Campetella, C. M., and N. E. Possia (2007), Upper-level cut-off lows in southern South America, *Meteorol. Atmos. Phys.*, *96*, 181–191.

de Abreu, R. C., and R. P. da Rocha (2015), Numerical experiments to the subtropical cyclone "Anita" using WRF model, *Ciencia Nat.*, *37*, 69–74.

Dee, D. P., et al. (2011), The ERA-Interim reanalysis: Configuration and performance of the data assimilation system, *Q. J. R. Meteorol. Soc.*, *137*, 553–597.

Dias Pinto, J. R., M. S. Reboita, and R. P. da Rocha (2013), Synoptic and dynamical analysis of subtropical cyclone Anita (2010) and its potential for tropical transition over the South Atlantic Ocean, *J. Geophys. Res. Atmos.*, *118*, 10,870–10,883, doi:10.1002/jgrd.50830.

Drumond, A., R. Nieto, L. Gimeno, and T. Ambrizzi (2008), A Lagrangian identification of major sources of moisture over Central Brazil and La Plata Basin, *J. Geophys. Res.*, *113*, D14128, doi:10.1029/2007JD009547.

Drumond, A., R. Nieto, R. Trigo, T. Ambrizzi, E. Souza, and L. Gimeno (2010), A Lagrangian identification of the main sources of moisture affecting northeastern Brazil during its pre-rainy and rainy seasons, *PLoS One*, *5*(6) e11205.

Drumond, A., J. Marengo, T. Ambrizzi, R. Nieto, L. Moreira, and L. Gimeno (2014), The role of the Amazon Basin moisture in the atmospheric branch of the hydrological cycle: A Lagrangian analysis, *Hydrol. Earth Syst. Sci.*, *18*, 2577–2598.

Durán-Quesada, A. M., M. S. Reboita, A. M. Ramos, R. P. da Rocha, R. Nieto and L. Gimeno (2010), Moisture variations during the life cycle of cyclones in the east coast of South America, in *Geophys. Res. Abstr.*, vol. 12, EGU2010-222-2, European Geosciences Union Assembly, Viena, Áustria.

Durán-Quesada, A. M., M. S. Reboita, and L. Gimeno (2012), Precipitation in tropical America and the associated sources of moisture: A short review, *Hydrol. Sci. J.*, *57*(4), 612–624.

Evans, J. L., and A. Braun (2012), A climatology of subtropical cyclones in the South Atlantic, *J. Clim.*, *25*, 7328–7340.

Evans, J. L. and M. P. Guishard (2009), Atlantic subtropical storms. Part I: Diagnostic criteria and composite analysis, *Mon. Weather Rev.*, *137*(7), 2065–2080.

Fernandez, J. P. R., S. H. Franchito, and V. B. Rao (2006), Simulation of the summer circulation over South America by two regional climate models. Part I: Mean climatology, *Theor. Appl. Climatol.*, *86*(1–4), 247–260.

Garde, L. A., A. B. Pezza, and J. A. T. Bye (2010), Tropical transition of the 2001 Australian Duck, *Mon. Weather Rev.*, *138*, 2038–2057.

Gimeno, L., A. Drumond, R. Nieto, R. M. Trigo, and A. Stohl (2010), On the origin of continental precipitation, *Geophys. Res. Lett.*, *37*, L13804, doi:10.1029/2010GL043712.

Gimeno, L., R. Nieto, A. Drumond, R. Castillo, and R. Trigo (2013), Influence of the intensification of the major oceanic moisture sources on continental precipitation, *Geophys. Res. Lett.*, *40*, 1443–1450, doi:10.1002/grl.50338.

Godoy, A. A., N. E. Possia, C. M. Campetella, and Y. G. Skabar (2011), A cut-off low in southern South America: Dynamic and thermodynamic processes, *Rev. Bras. Meteorol.*, *26*, 503–514.

González-Alemán, J. J., F. Valero, F. Martín-León, and J. L. Evans (2015), Classification and synoptic analysis of subtropical cyclones within the northeastern Atlantic Ocean, *J. Clim.*, *28*(8), 3331–3352.

Gozzo, L. F., and R. P. da Rocha (2013), Air-sea interaction processes influencing the development of a Shapiro-Keyser type cyclone over the subtropical South Atlantic Ocean, *Pure Appl. Geophys.*, *170*(5), 917–934.

Gozzo, L. F., R. P. da Rocha, M. S. Reboita, and S. Sugahara (2014), Subtropical cyclones over the southwestern South Atlantic: Climatological aspects and case study, *J. Clim.*, *27*, 8543–8562.

Guishard, M. P., J. L. Evans, and R. E. Hart (2009), Atlantic subtropical storms. Part II: Climatology, *J. Clim.*, *22*, 3574–3594.

Hart, R. E. (2003), A cyclone phase space derived from thermal wind and thermal asymmetry, *Mon. Weather Rev.*, *131*, 585–616.

Herdies, D. L., A. da Silva, M. A. Silva Dias and R. Nieto-ferreira (2002), Moisture budget of the bimodal pattern of the summer circulation over South America, *J. Geophys. Res.*, *107*(D20), 8075, doi:10.1029/2001JD000997.

Hong, S.-Y., Y. Noh, and J. Dudhia (2006), A new vertical diffusion package with an explicit treatment of entrainment processes, *Mon. Weather Rev.*, *134*, 2318–2341.

Janjic, Z. I. (1994), The step-mountain Eta coordinate model: Further developments of the convection, viscous sublayer and turbulence closure schemes, *Mon. Weather Rev.*, *122*, 927–945.

Kuo, Y. H., R. J. Reed, and S. Low-nam (1991), Effects of surface energy fluxes during the early development and rapid intensification stages of seven explosive cyclone in the western Atlantic, *Mon. Weather Rev.*, *119*, 457–476.

Lee, C. S. (1989), Observational analysis of tropical cyclogenesis in the western North Pacific. Part II: Budget analysis, *J. Atmos. Sci.*, *46*(16), 2599–2616.

Liberato, M. L., A. M. Ramos, R. M. Trigo, I. F. Trigo, A. M. Durán-quesada, R. Nieto, and L. Gimeno (2013), Moisture sources and large-scale dynamics associated with a flash flood event, *Lagrangian Model. Atmos.*, 111–126.

Marengo, J. A., W. R. Soares, C. Saulo, and M. Nicolini (2004), Climatology of the low-level jet east of the Andes as derived from the NCEP-NCAR reanalyses: Characteristics and temporal variability, *J. Clim.*, *17*(12), 2261–2280.

Mathias, R. S. B. (2012), Análise e classificação de ciclones utilizando diagramas de fase: Conceitos e aplicação em previsão do tempo operacional, Dissertação (Mestrado em Meteorologia) - Centro de Ciências Matemáticas e da Natureza – UFRJ, 117 pp.

McTaggart-Cowan, R., L. F. Bosart, C. A. Davis, E. H. Atallah, J. R. Gyakum, and K. A. Emanuel (2006), Analysis of Hurricane Catarina (2004), *Mon. Weather Rev.*, *134*, 3029–3053.

Monin, A. S. and A. M. Obukhov (1954), Basic laws of turbulent mixing in the surface layer of the atmosphere. *Contrib. Geophys. Inst. Acad. Sci.*, USSR, *151*, 163–187.

Nieto, R., L. Gimeno, and R. M. Trigo (2006), A Lagrangian identification of major sources of Sahel moisture, *Geophys. Res. Lett.*, *33*, L18707, doi:10.1029/2006GL027232.

Numaguti, A. (1999), Origin and recycling processes of precipitating water over the Eurasian continent: Experiments using an atmospheric general circulation model, *J. Geophys. Res.*, *104*(D2), 1957–1972.

Ordóñez, P., M. L. Liberato, J. G. Pinto and R. M. Trigo (2013), Analysis of moisture advection during explosive cyclogenesis over North Atlantic Ocean, in *EGU General Assembly Conference Abstracts*, vol. 15, p. 8452.

Pereira-filho, A. J., A. B. Pezza, I. Simmonds, R. S. Lima, and M. Vianna (2010), New perspectives on the synoptic and mesoscale structure of Hurricane Catarina, *Atmos. Res.*, *95*, 157–171.

Piva, E., M. A. Gan, and M. C. L. Moscati (2011), The role of latente and sensible heat fluxes in an explosive cyclogenesis over South America east coast, *J. Meteorol. Soc. Jpn.*, *89*, 637–663.

Reboita, M. S., R. P. da Rocha, T. Ambrizzi, and E. Caetano (2010), An assessment of the latent and sensible heat flux on the simulated regional climate over southwestern South Atlantic Ocean, *Clim. Dyn.*, *34*, 873–889.

Reboita, M. S., R. P. da Rocha, and T. Ambrizzi (2012), Dynamic and climatological features of cyclonic developments over southwestern South Atlantic Ocean, *Horizonts Earth Sci. Res.*, *6*, 135–160.

Silva, M. C. L. (2014), Simulações Numéricas do Ciclone Catarina: Impacto dos Efeitos Subgrade, Resolução e Assimilação de Dados, Tese (Doutorado em Meteorologia) – IAG-USP, 98 pp.

Silva, G. A. M., A. Drumond, and T. Ambrizzi (2011), The impact of El Niño on South American summer climate during different phases of the Pacific Decadal Oscillation, *Theor. Appl. Climatol.*, *106*(3–4), 307–319.

Skamarock, W. C., et al. (2008), A description of the Advanced Research WRF Version 3, NCAR Technical Note NCAR/TN–475+STR, Boulder, Colo.

Sodemann, H., C. Schwierz, and H. Wernli (2008), Interannual variability of Greenland winter precipitation sources: Lagrangian moisture diagnostic and North Atlantic Oscillation influence, *J. Geophys. Res.*, *113*, D03107, doi:10.1029/2007JD008503.

Stohl, A., and P. James (2004), A Lagrangian analysis of the atmospheric branch of the global water cycle. Part I: Method description, validation, and demonstration for the August 2002 flooding in Central Europe, *J. Hydrometeorol.*, *5*, 656–678.

Stohl, A., C. Forster, A. Frank, P. Seibert, and G. Wotawa (2005), Technical note: The Lagrangian particle dispersion model FLEXPART version 6.2, *Atmos. Chem. Phys.*, *5*, 2461–2474.

Tao, W.-K., J. Simpson, and M. McCumber (1989), An ice-water saturation adjustment, *Mon. Weather Rev.*, *117*, 231–235.

Trenberth, K. E., and C. J. Guillemot (1998), Evaluation of the atmospheric moisture and hydrological cycle in the NCEP/NCAR reanalyses, *Clim. Dyn.*, *14*(3), 213–231.

Trenberth, K. E., J. T. Fasullo, and J. Mackaro (2011), Atmospheric moisture transports from ocean to land and global energy flows in reanalyses, *J. Clim.*, *24*, 4907–4924.

Veiga, J. A. P., A. B. Pezza, I. Simmonds, and P. L. Silva Dias (2008), An analysis of the environmental energetics associated with the transition of the first South Atlantic hurricane, *Geophys. Res. Lett.*, *35*, L15806, doi:10.1029/2008GL034511.

Vera, C., J. Baez, M. Douglas, and C. B. Emmanuel (2006), The south American low-level jet experiment, *Bull. Am. Meteorol. Soc.*, *87*(1), 63.

Vianna, M. L., V. V. Menezes, A. B. Pezza, and I. Simmonds (2010), Interactions between Hurricane Catarina (2004) and warm core rings in the South Atlantic Ocean, *J. Geophys. Res.*, *115*, C07002, doi:10.1029/2009JC005974.